

Proof of concept for a lightweight panel with enhanced sound absorption exploiting rainbow labyrinthine metamaterials

V. Hasanuzzaman Kamrul¹, L. Bettini¹, E. Musso¹, F. Nistri^{1, 2}, D. Piciuccio¹, M. Zemello¹, A.O. Krushynska³, D. Misseroni⁴, N. Pugno⁴, M. Lott², A.S. Gliozzi², L. Shtrepi⁵, and F. Bosia^{2, †}

¹*Politecnico di Milano, Milano, Italy*

²*DISAT, Politecnico di Torino, Torino, Italy*

³*University of Groningen, Groningen, The Netherlands*

⁴*University of Trento, Trento, Italy*

⁵*DENERG, Politecnico di Torino, Torino, Italy*

[†]*Corresponding author: federico.bosia@polito.it*

Abstract

In this work, we demonstrate in a proof of concept experiment the efficient noise absorption of a 3-D printed panel designed with appropriately arranged space-coiled labyrinthine acoustic elementary cells. The labyrinthine units are numerically simulated to determine their dispersion characteristics and then experimentally tested in a Kundt Tube to verify the dependence of absorption characteristics on cell thickness and lateral size. The resonance frequency is found to scale linearly with respect to both thickness and lateral size in the considered range, enabling tunability of the working frequency. Using these data, a flat panel is designed and fabricated by arranging cells of different dimensions in a quasi-periodic lattice, exploiting the acoustic “rainbow” effect, i.e. superimposing the frequency response of the different cells to generate a wider absorption spectrum, covering the required frequency range between 800 and 1200 Hz. The panel is thinner and more lightweight compared to other sound absorption solutions, and designed in modular form so as to be applicable to different geometries. The performance of the panel is experimentally validated in a small-scale reverberation room, and close to ideal absorption is demonstrated at the desired frequency of operation. Thus, this work suggests a design procedure for noise-mitigation panel solutions and provides experimental proof of the versatility and effectiveness of labyrinthine metamaterials for low-frequency sound attenuation.

Introduction

In the past years, Acoustic Metamaterials (AMs) have gained widespread attention because of their exceptional properties, which are not commonly found in naturally occurring materials. AMs could potentially pave the way to the development of a new generation of absorbers and diffusers with deep-subwavelength thickness, that can be tailored for a desired frequency spectrum [1]. Their use brings new possibilities into the traditional problem of achieving low-frequency absorption. In addition, AMs offer the possibility to achieve a high level of performance, or noise attenuation, compatibly with reduced size and weight characteristics.

Roughly speaking, it is possible to distinguish three classes of AMs [2]–[4]: membrane-type AMs, AMs with scatterers, and labyrinthine (or cavity-based) AMs [1]. While the performance of the first two classes are often tuned and/or improved by the synergy with conventional acoustic absorbers (e.g. porous materials [5], [6], heavy resonators [7], Helmholtz resonators [8] or tensioned membranes), labyrinthine AMs can provide a breakthrough in achieving acoustic absorption without integration of further technologies. Indeed, labyrinthine MMs offer several advantages within the same domain of MMs, as other MM-based solutions (e.g., tensioned membrane MMs) lack structural rigidity and their resonance frequency suffers from instabilities due to change in material prestress, thus making it difficult controlling low-frequency sound waves.

First proposed by Liang and Li [9], labyrinthine metamaterials are based on realizing a coiled wave propagation space using curved channels, whose substantial phase delays enable to decrease the effective speed of acoustic waves. This can be interpreted as an increase of the effective refractive index. Equivalent refractive indexes of $n_D \gg 1$ for waves confined in curled channel have been reported in previous works [10]–[12].

The physical mechanism enabling sound attenuation in labyrinthine AMs is based on collective resonances (i.e. Mie resonances) that produce total reflections over broad frequency ranges [12]. This mechanism differs from what occurs in conventional absorbers, where sound wave propagation or attenuation properties depend on the channel width. In the case of narrow channels, friction and thermo-viscous effects in the vicinity of the channel walls inhibit wave propagation and lead to its total attenuation [13]. In the case of medium-sized channels, if the sound wavelength matches the distance between the two channel edges (i.e., it equals an integer number of half wavelengths) amplification of the sound transmission can occur at the corresponding frequency.

Labyrinthine metastructures allow to tune operating frequencies to desired ranges by only varying the internal channel thickness and length [14]. Other studies suggest that resonances within the straight slits of space-filling curves govern the generation of acoustic band gaps [15]. This mechanism does not exploit thermo-viscous dissipation losses in air, as in e.g. porous foams, and achieves sound absorption by means of a purely resonant mechanism. Tuning other structural and design parameters (e.g., by increasing the channel tortuosity, or further elongating the wave path), it is possible to achieve almost perfect

reflection at band gap frequencies.

For this reason, labyrinthine AMMs exhibit remarkable properties with regimes of total transmission and total reflection, which can be adapted for low frequency sound control simply by varying cavity size, while other geometric parameters remain unchanged.

This kind of adaptability could largely benefit noise absorption applications at small to medium scale, where restrictions on structural size of the absorbers impose trade-offs between efficiency and encumbrance. Sufficiently thick conventional acoustic absorbing materials, such as those used in anechoic chambers, can absorb acoustic waves in wide frequency ranges, but their bulky characteristics limit their broad application. In this regard, an optimally integrated acoustic resonator structure can provide the advantage of being able to target a specific noise spectrum range, with a reduced sample thickness [16]. This can lead to potentially attractive implementations in lightweight acoustic barriers with enhanced broadband wave-reflecting performance. Moreover, the weight characteristics become crucial when dealing with devices in the aerospace industry.

At present, there are limitations related to sample production costs that affect testing procedures of these materials. These are usually limited to Impedance Tube measurements in terms of transmission loss (TL) or normal incidence sound absorption coefficients (α_0). Therefore, it is important to investigate AM performance in more realistic conditions, i.e. in diffuse field conditions.

This work presents a proof of concept experiment to demonstrate efficient noise absorption of a 3-D printed panel designed with appropriately arranged space-coiled labyrinthine acoustic elementary cells. Numerical simulation are used to determine their dispersion characteristics and experimental tests in a Kundt Tube to verify the dependence of absorption characteristics on cell thickness and lateral size. Finally, the performance of the panel is experimentally validated in a small-scale reverberation room.

1 Methods

1.1 Sample design and manufacturing

In order to assess the efficiency of sound wave absorption at subwavelength scale, we perform normal incidence measurements on various types of the Acoustic Elementary Cells (AECs). The AECs consist of a squared cavity inside a solid cylinder, inside which internal solid walls form a labyrinthine pattern. The samples are depicted in Fig. 1. We studied three types of labyrinthine geometries. The first, proposed in [14] is a circular spider web-structured labyrinthine geometry embedded in a square cavity. The second and the third correspond to the first-iteration and second-iteration Wunderlich curves, respectively, whose attenuation properties have been numerically studied in [15].

The AECs for impedance tube measurements were manufactured at the Politecnico di Torino using a Dremel Digilab filament 3D printer (PLA) and at

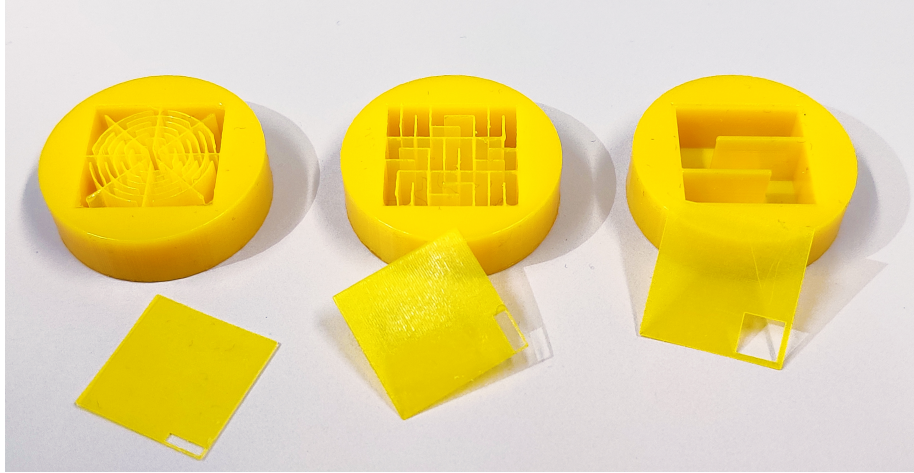


Figure 1: Tested labyrinthine AEC samples.

the University of Trento using a Stratasys J750 FDM 3D printer (VeroYellow polymer). The printed elementary cells feature thin removable apertures of either square or rectangular shapes on the face exposed to wave normal incidence (see Fig. 1). Therefore, the aperture surface determines the sound pressure amplitude in the cavity.

1.2 Impedance tube measurements

The impedance tube setup is depicted in Fig. 2. The impedance measurements were performed in agreement with ISO 10534-2 [17] and ASTM E1050-19 [18] (two-microphone technique) regulations, in order to measure the normal-incidence absorption coefficient α_0 and the sound transmission loss (STL) [19] for the three filtering structures. This procedure provides the possibility of directly measuring small samples suitable for the applications considered in this investigation.

Measurements were performed in the Applied Acoustics Laboratory, Politecnico di Torino, using a HW-ACT-TUBE and -STL (Siemens, Munich, Germany), which has a diameter of 35 mm and is equipped with two $\frac{1}{4}$ " flush mounted GRAS 46BD (GRAS, Holte, Denmark, see Fig. 2C). The method allows to obtain accurate sound pressure amplitude and phase measurements in the whole frequency range of interest, i.e., 100-5000 Hz [19].

The geometry of the tube follows the specifications of both ASTM and ISO standards, including the minimum distance between microphone and source, and microphone and test sample. The impedance tube has been equipped with three microphone holders to extend as much as possible the supported frequency range. Therefore, it is possible to obtain accurate measurements in a low frequency range of 50 to 2400 Hz and at high frequency range of 119 to 5700 Hz when a 65 mm and a 29 mm microphone spacing is used, respectively (Fig. 2B).

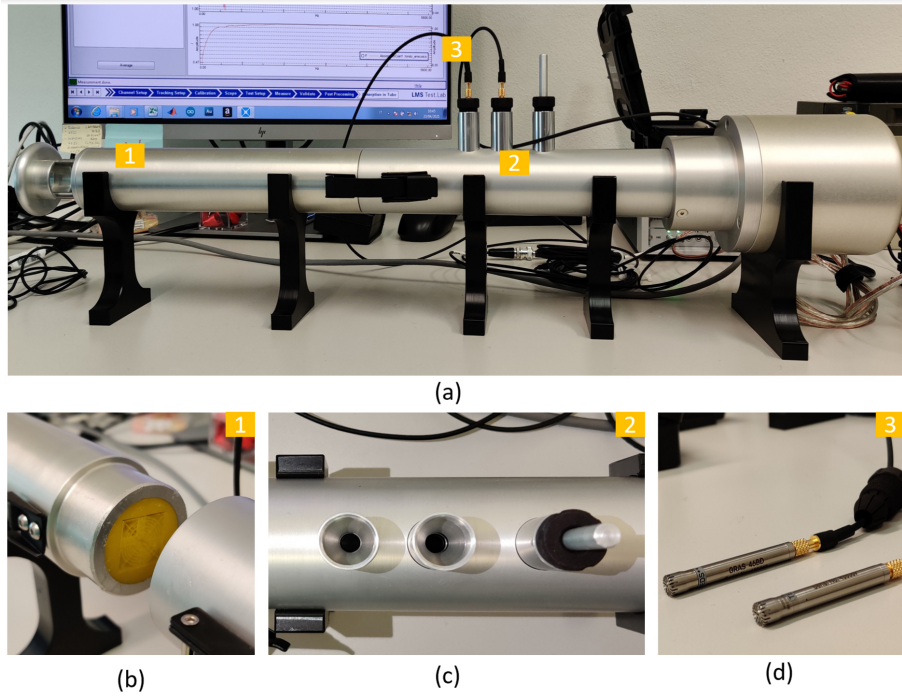


Figure 2: **Experimental setup for impedance tube measurements.** (a) The complete impedance tube. (b) The sample holder consists of a tube with a rigid piston and the AEC sample can be mounted inside the cavity; (c) Openings for microphone insertion; (d) The two employed $\frac{1}{4}$ " flush mounted GRAS 46BD microphones.

A white noise source, i.e., a 2" aluminium driver, integrated in the system is capable of producing continuous high sound levels (100 dB) inside the tube, assuring a high signal to noise ratio by design and generating a flat spectrum in the 100-5000 Hz frequency range. The sample holder consists of a tube with a sliding rigid piston. A specific plastic sample holder was used as shown in (Fig. 2A). The method allowed better control on the positioning of the different samples into the flanged-to-sample holder of the tube. The 3D printed samples have a reflective overall surface and a diameter allowing for tolerances such that the circumferential effect discussed in [20] could be considered negligible. The effect of any possible irregularity in the samples, and in particular at the edges, was taken into consideration by repeating the tests for each structure with three (nominally equal) samples in order to evaluate reproducibility. Temperature and atmospheric pressure were monitored by calibrated transducers.

1.3 Small scale reverberation room (SSRR)

The measurement of the complete sound absorption panel was performed in the small-scale reverberation room at the Politecnico di Torino. A full validation

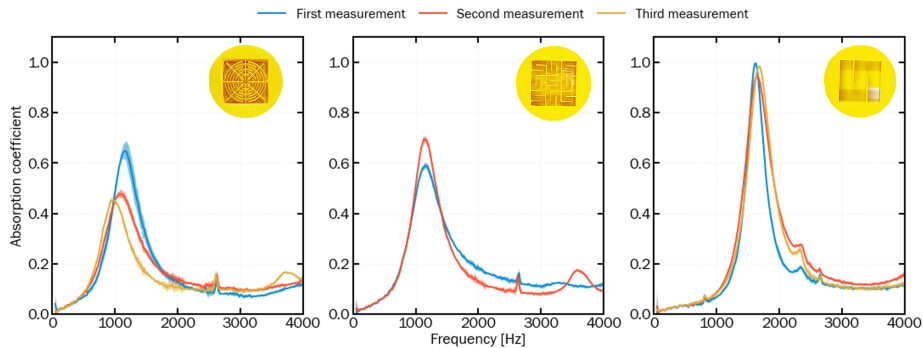


Figure 3: . **Averaged absorption spectra for the three proposed AEC structures.** From left to right, the absorption spectra of the spider-web labyrinthine AEC, the second-iteration Wunderlich curve and the first- iteration Wunderlich curve. Each color corresponds to a different experimental configuration. Shaded areas correspond to standard deviations calculated over repeated measurements of each configuration.

of the room is presented in [21], highlighting the 400-5000 Hz general validity frequency range. Depending on the material, this can be extended also at lower frequencies (≈ 250 Hz).

The room is an oblique angled room with nonparallel walls. It has a floor area of about 2.38 m^2 , total area of 12.12 m^2 and a volume of 2.86 m^3 . The structure is raised from the ground on a wooden structure and damping layers have been used along the joints and openings. One of the sides consists of two movable parts that provide a large opening for the positioning of the sample. The construction material is self-supporting lightweight partitions of Medium Density Fibreboard (MDF) with a thickness of 3.8 cm , which has been further covered by a layer of adhesive film in order to maximize its reflective properties. The average absorption coefficient of the indoor surfaces is lower than $\alpha_m = 0.05$ in the frequency range of interest (100-5000 Hz). The mean reverberation time of the empty room between 100 Hz and 5000 Hz is of 0.95 s , so that the Schroeder frequency f_s is 1152 Hz .

In order to ensure a high diffusivity of the sound field, 8 diffusers (13.5% of the total room area) have been hung on the ceiling after a diffusivity check in accordance with ISO 354, based on the measurements of the mean absorption coefficient (500-5000 Hz). The procedure consists in using the integrated impulse response method [17] for simultaneous measurements on six different microphone positions in two conditions, i.e. with and without the sample on the floor of the room.

The measurement chain includes a set-up of six $1/4''$ BSWA Tech MPA451 microphones and ICP104 (BSWA Technology Co., Ltd., Beijing, China); two ITA High-Frequency Dodecahedron Loudspeakers with their specific ITA power amplifiers (ITA-RWTH, Aachen, Germany) and a sound card Roland Octa-Capture UA-1010 (Roland Corporation, Japan) in order to perform 12 measurements (the minimum number required by ISO 354 [17]). We used a MATLAB

code combined with the functions of the ITA-Toolbox (an opensource toolbox from RWTH-Aachen, Germany) for sound generation, recording and signal processing.

For the entire frequency range, the sound pressure levels in the room were less than 6 dB in adjacent one-third-octave bands. On the other hand, only above 250 Hz the excitation signal level before its decay was sufficiently high so that the lower dB threshold was at least 10 dB above the background noise level (i.e., 35 dB below the initial sound pressure level). Therefore, the sound source fulfils the ISO 354 spectral characteristics only above 250 Hz.

We arranged the experimental set-up in agreement with the recommendations of the ISO 354 standard, resized accordingly due to the 1:5 scale. Thus, we positioned the microphones at 0.3 m distance from each other, 0.2 m from the room surfaces and 0.4 m from the sources. The two sources were 0.6 m apart. The distance between the sample sides was greater than 0.2 m. We performed a spatial averaging considering all the 12 sources and microphones combinations, checking the temperature (≥ 15 °C) and humidity (between 30-90 %) conditions

1.4 Measurement procedure of the acoustic panel

In accordance with ISO 354, before measurements we calculated the equivalent specimen absorption area, which is given, in square meters, by the formula

$$A_T = 55.3V \left(\frac{1}{c_2 T_2} - \frac{1}{c_1 T_1} \right) - 4V(m_2 - m_1) \quad (1)$$

where T_1, T_2 are the reverberation times (in s) of the reverberation room without and with the specimen, respectively; V is the volume of the empty reverberation room, in m^3 ; c_1, c_2 are the sound propagation speeds in air in the SSRR without and with the sample, respectively; m_1, m_2 are the power attenuation coefficients of the climatic conditions in the reverberation room without and with the sample.

The test procedure consisted in using the integrated impulse response method, in which the filtered impulse response to a test signal is backward integrated. This allows to evaluate the decay times for each frequency band. The reverberation times of the room in each frequency band are then expressed by the arithmetic mean of the total number of reverberation time measurements made in that frequency band. The two values are then used in order to compute. Finally, the random-incidence absorption coefficient of the tested specimen is computed as

$$\alpha = \frac{A_T}{S} \quad (2)$$

Where S is the area covered by the test specimen, expressed in m^2 .

2 Results and discussion

2.1 Comparison between different AEC geometries

The aforementioned impedance tube has a spectral resolution of 2 Hz over a frequency range extending from 50 Hz to 5700 Hz. We performed repeated measurements on each AEC, in order to assess reproducibility and repeatability. Each measurement followed a fixed protocol: first, we set up the experiment by placing the AEC in the impedance tube sample holder. Once fixed, the stability of environmental conditions allows to characterize reproducibility. The sound pressure level at specific locations along the length of the tube are measured and the absorption coefficient spectrum of the AEC $\alpha(f)$, obtained as

$$\alpha = 1 - \frac{W_r}{W_t}, \quad (3)$$

where W_r and W_t are the reflected and total power. Repeating the latter operation several times for a fixed experimental configuration allows to characterize repeatability.

A resonance-based metamaterial with non-vanishing dissipation is characterized by an absorption spectrum following a Lorentzian curve,

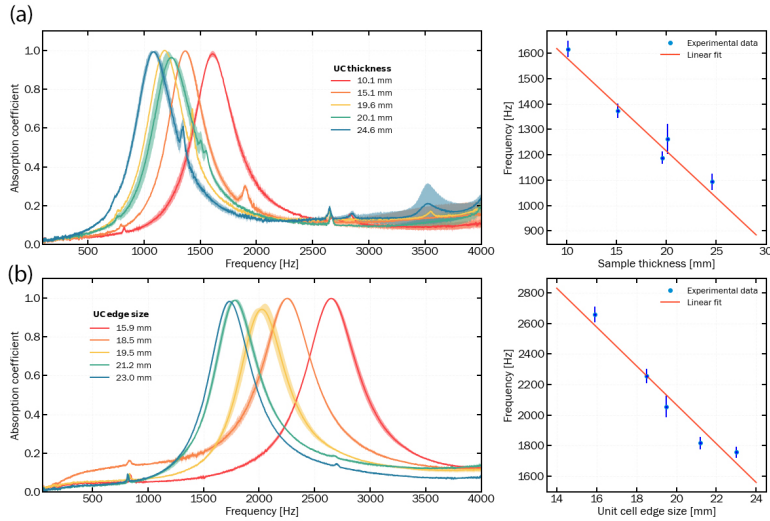


Figure 4: **Averaged absorption spectra of first-iteration Wunderlich curve AECs with varying lateral size and thickness.** The resonance frequency displays a linear decrease both when the AEC thickness (top) and the UC size (bottom) increase.

$$\mathcal{L}(\alpha, f_r, \Delta f) = \alpha \frac{\Delta f^2}{4(f - f_r)^2 + \Delta f^2}, \quad (4)$$

where α is the absorption coefficient, normalized over the amplitude of the pressure wave, f_r is the resonance frequency and Δf the resonance bandwidth.

In Fig. 3, the measured absorption spectra for three labyrinthine AECs are shown. The tested samples had a UC lateral size of 15.5 mm (i.e., the edge of the square cavity in Fig. 1) and a thickness of 9.6 mm. Their absorption spectra exhibit a clear resonant peak at different resonance frequencies. However, the quality of the curve and the reproducibility of the measurements are different in the three cases. Both the spider-web circular structure and the second-iteration Wunderlich curve feature are characterized by an absorption coefficient below 70% and scarce reproducibility. On the other hand, the first-iteration Wunderlich curve features both good reproducibility and an excellent absorption coefficient $\alpha = (97.4 \pm 0.5)\%$ at a frequency $f_r = (1665 \pm 25)$ Hz.

The low Q-factor resonance curves in the first two cases could be due to their internal channel widths being too narrow to neglect viscoelastic effects. Moreover, because the aperture size of these AECs is smaller (see Fig. 1), diffraction of acoustic waves at the entrance lead to peak enlargement. Therefore, the aperture size plays a role in the amplitude and the bandwidth of the absorption peak, but not on the absorption properties of the MM structure.

2.2 AEC resonance frequency tunability

After the preliminary assessment of the first-iteration Wunderlich curve's absorption properties, the resonance frequency dependence on the size of the AEC cavity was studied. In resonance-based metamaterials, the absorption frequency can be changed by modifying the AEC unitary cell edge size and scaling the channel width accordingly [14]. Similarly, the resonance frequency depends on the AEC thickness in the normal direction.

In order to quantify the resonance frequency dependence on the geometrical size, we manufactured several AECs similar to the ones in Fig. 1, but varying both their thicknesses (within the 10-25 mm range, keeping their UC edge size fixed to 21.2 mm) and their UC edge size (within the 15-23.0 mm range, keeping their thickness fixed to 12.6 mm). Results are shown in Fig. 4.

The resonance frequency scales linearly by a factor $\frac{df_r}{dz} = (-42.7 \pm 1.0)$ Hz mm^{-1} with the sample thickness z , and by a factor $\frac{df_r}{dl} = (-145.3 \pm 8.0)$ Hz mm^{-1} with the AEC edge size l . Thus, the influence of the AEC lateral size allows to tune the working frequency in a larger interval, while the thickness dependency can be employed to fine-tune more specifically the frequency to the desired value.

2.3 Rainbow-based AMM panel design and fabrication

Using impedance tube data relative to the characterization of the chosen AEC, we establish the objective of sound absorption in a chosen low-frequency range of interest e.g. for aeronautics, between 800 and 1200 Hz. This can be achieved by exploiting various AECs of different lateral sizes and thicknesses, so that

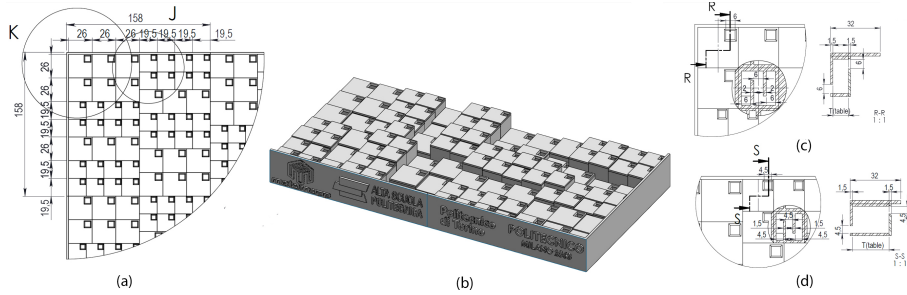


Figure 5: **Modular elements of the complete sound absorption panel.** (a) Top view of the macro-cell, showing its geometrical size; (b) Two adjacent macro-cells. Each macro-cell consists of several AECs of edge size l_1 and l_2 with varying thicknesses. Adjacent macro-cells are reflected and rotated by 90° in order to guarantee a globally homogeneous spectral response. (c)-(d) Technical drawings of the 26 mm AEC and the 19.5 mm edge AEC, respectively. The thicknesses of the internal walls are different in the two cases.

the resulting resonance spectrum is given by their superposition, and the corresponding absorption range extends over the desired range.

An AM panel was thus designed. The panel consists of differently sized AECs, with varying thicknesses and areas. The internal walls thickness of each AEC is proportional to the AEC edge area. Starting from two AEC edge sizes ($l_1 = 19.5$ mm and $l_2 = 26$ mm) at different thicknesses ($t_1 = 10 \div 15$ mm for the l_1 AEC, and $t_2 = 23 \div 25$ mm for the l_2 AEC), a spatial pattern of repeated l_1 and l_2 AECs was conceived, covering a total module of 156×156 mm² area.

We define this module “macro-cell” because of its intermediate size between an AEC and the complete sound absorbing panel. In fact, the complete panel consists of the juxtaposition of 20 macro-cells arranged in the plane, to cover a total surface of 628×784 mm², i.e., the area of the panel. Adjacent macro-cells are rotated by 90 degrees and reflected, (Fig. 5) to ensure maximum spatial homogeneity in the sound absorbing properties.

The polyamide panel was manufactured through selective laser sintering (SLS), a technique where each level is sintered by a laser beam, directed by a scanning system. The process is repeated, and the prototype is built layer by layer. SLS does not require supports to sustain oblique and horizontal protrusions and it allows to fabricate undercuts. However, for manufacturing hollow structures like the AECs, it is necessary to include at least two holes (on top and bottom surfaces) for each labyrinth cavity, in order to remove any residual powder, so one additional opening was added for each AEC. For the measurement phase, these additional openings were covered with properly sized polyamide caps which were fixed with aluminum tape to guarantee an acoustic seal. The finished panel is shown in 6.

2.4 Metamaterial panel testing in a reverberation chamber

The panel absorption properties were measured by comparing its absorption spectrum with and without admitting sound waves within the AECs cavities. As shown in Fig. 5, the panel has a flat and an uneven upper surface. The lower flat surface presents the apertures from which the sound waves are admitted into the AEC. On the contrary, the uneven surface is fully sealed, and sound waves can neither enter nor exit from it.

Fig. 6 displays the experimental test configuration of the panel: the flat surface is facing the sound source. This configuration corresponds to the device in operation. On the other hand, when the panel presents the uneven, closed

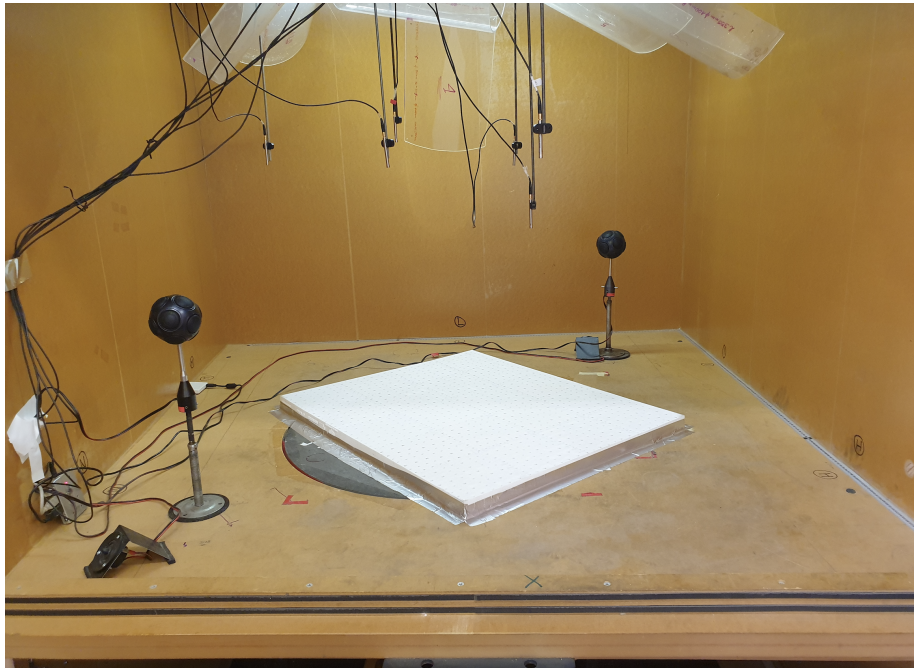


Figure 6: Measurement of the metamaterial panel in the SSRR.

face towards the sound source, sound waves do not propagate into the AECs, and the intrinsic absorption properties of the polyamide panel without MMs can be assessed.

Measuring the panel in the two configurations allows the derivation of the MM-induced absorption enhancement. In Fig. 7, the comparison of the absorption spectrum in the two configurations is shown. Frequencies of interest are reported as third-octave bands in the range of interest (250-5000 Hz). The blue line shows the intrinsic absorption of the uneven polyamide surface, while the red line shows evidence of an effective broadband sound absorption, close

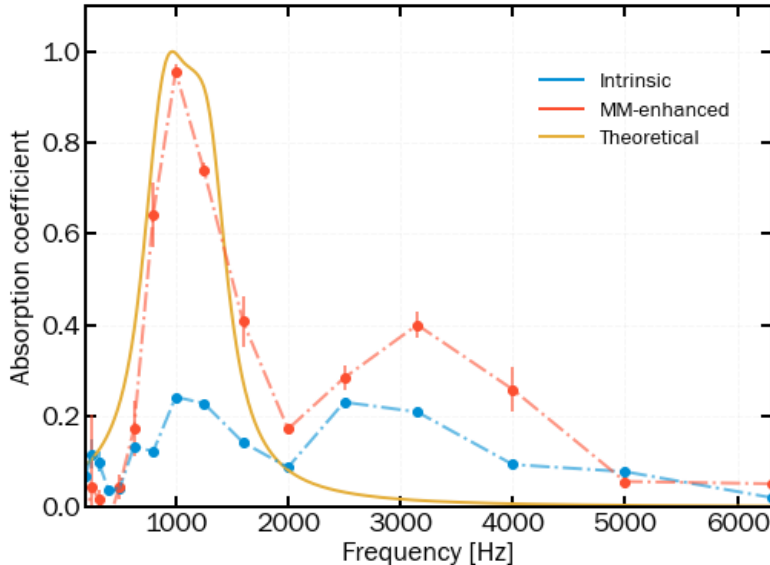


Figure 7: **Absorption spectrum of the SSRR measurement of the panel.** The comparison between the MM-enhanced and the intrinsic polyamide absorption is plotted.

to the ideal value of 1, occurring between 800 and 1300 Hz, i.e., in the expected frequency range. The theoretical broadband absorption curve (yellow) is computed as the average absorption spectrum of many lorentzian lineshapes (Eq. 2.1) peaked around the resonance values inferred from the linear fits of Fig. 4. For each lorentzian, we considered an average bandwidth $\Delta f = 400$ Hz, coherently with the prior measurements.

3 Conclusions

In this work, we have provided an experimental proof of concept for a novel approach to noise attenuation exploiting a rainbow-based design using labyrinthine metamaterials and combining AECs of varying thickness and lateral size in a quasi-periodic arrangement that ensured good homogeneity in the panel response. We have described the full design and validation procedure, from numerical modeling of the unit cell, to its characterization in an impedance tube, to the design of the macrocells composing the panel, and its realization using selective laser sintering. The final structure has then been characterized experimentally in a reverberation chamber, demonstrating a close to ideal absorption over the targeted low frequency range, centred at 1 kHz, thus validating the approach. The proposed prototype can be further developed, and thanks to its modular design, can be employed in diverse applications, e.g. in room acoustics, in automotive parts, or aeronautics in general. Overall, we have proposed an alternative (or complementary) route to the use of traditional sound insulation

materials in noise control. The proposed solution can be particularly attractive due to the small thicknesses and low density of the required parts emerging from the subwavelength nature of the labyrinthine metamaterials used in the design.

Acknowledgements

VHK, LB, EM, FN, DP, MZ, ASG, LS, FB thank the Alta Scuola Politecnica project “MetaMAPP”.

ASG, FB are supported by H2020 FET Open “Boheme” grant No. 863179.

References

- [1] X. Zhang, Z. Qu, and H. Wang, “Engineering Acoustic Metamaterials for Sound Absorption: From Uniform to Gradient Structures,” *iScience*, vol. 23, no. 5, 2020, ISSN: 25890042. DOI: 10.1016/j.isci.2020.101110.
- [2] M. I. Hussein, M. J. Leamy, and M. Ruzzene, “Dynamics of Phononic Materials and Structures: Historical Origins, Recent Progress, and Future Outlook,” *Applied Mechanics Reviews*, vol. 66, no. 4, 2014, ISSN: 0003-6900. DOI: 10.1115/1.4026911.
- [3] B. Assouar, B. Liang, Y. Wu, Y. Li, J.-C. Cheng, and Y. Jing, “Acoustic metasurfaces,” *Nature Reviews Materials*, vol. 3, no. 12, 2018, ISSN: 2058-8437. DOI: 10.1038/s41578-018-0061-4.
- [4] H. Ge, M. Yang, C. Ma, M.-H. Lu, Y.-F. Chen, N. Fang, and P. Sheng, “Breaking the barriers: advances in acoustic functional materials,” *National Science Review*, vol. 5, no. 2, 2018, ISSN: 2095-5138. DOI: 10.1093/nsr/nwx154.
- [5] H. Meng, J. Wen, H. Zhao, L. Lv, and X. Wen, “Analysis of absorption performances of anechoic layers with steel plate backing,” *The Journal of the Acoustical Society of America*, vol. 132, no. 1, 2012, ISSN: 0001-4966. DOI: 10.1121/1.4728198.
- [6] T. Weisser, J.-P. Groby, O. Dazel, F. Gaultier, E. Deckers, S. Futatsugi, and L. Monteiro, “Acoustic behavior of a rigidly backed poroelastic layer with periodic resonant inclusions by a multiple scattering approach,” *The Journal of the Acoustical Society of America*, vol. 139, no. 2, 2016, ISSN: 0001-4966. DOI: 10.1121/1.4940669.
- [7] A. C. Slagle, “Low frequency noise reduction using novel poro-elastic acoustic metamaterials,” 2015.
- [8] Z. Liu, X. Zhang, Y. Mao, Y. Y. Zhu, Z. Yang, C. T. Chan, and P. Sheng, “Locally resonant sonic materials,” *Science*, vol. 289, 5485 2000, ISSN: 0036-8075. DOI: 10.1126/science.289.5485.1734.
- [9] Z. Liang and J. Li, “Extreme acoustic metamaterial by coiling up space,” *Physical Review Letters*, vol. 108, 11 Mar. 2012, ISSN: 0031-9007. DOI: 10.1103/PhysRevLett.108.114301.
- [10] T. Frenzel, J. D. Brehm, T. Buckmann, R. Schittny, M. Kadic, and M. Wegener, “Three-dimensional labyrinthine acoustic metamaterials,” *Applied Physics Letters*, vol. 103, 6 Aug. 2013, ISSN: 0003-6951.
- [11] J. Liu, L. Li, B. Xia, and X. Man, “Fractal labyrinthine acoustic metamaterial in planar lattices,” *International Journal of Solids and Structures*, vol. 132-133, Feb. 2018, ISSN: 00207683.
- [12] Y. Cheng, C. Zhou, B. G. Yuan, D. J. Wu, Q. Wei, and X. J. Liu, “Ultra-sparse metasurface for high reflection of low-frequency sound based on artificial mie resonances,” *Nature Materials*, vol. 14, 10 Oct. 2015, ISSN: 1476-1122.

- [13] M. Molerón, M. Serra-Garcia, and C. Daraio, “Visco-thermal effects in acoustic metamaterials: From total transmission to total reflection and high absorption,” *New Journal of Physics*, vol. 18, 3 Mar. 2016, ISSN: 1367-2630. DOI: 10.1088/1367-2630/18/3/033003.
- [14] A. O. Krushynska, F. Bosia, M. Miniaci, and N. M. Pugno, “Spider web-structured labyrinthine acoustic metamaterials for low-frequency sound control,” *New Journal of Physics*, vol. 19, 10 Oct. 2017, ISSN: 1367-2630. DOI: 10.1088/1367-2630/aa83f3.
- [15] A. O. Krushynska, F. Bosia, and N. M. Pugno, “Labyrinthine acoustic metamaterials with space-coiling channels for low-frequency sound control,” *Acta Acustica united with Acustica*, vol. 104, 2 Mar. 2018, ISSN: 1610-1928. DOI: 10.3813/AAA.919161.
- [16] J. Li, X. Wen, and P. Sheng, “Acoustic metamaterials,” *Journal of Applied Physics*, vol. 129, 17 May 2021, ISSN: 0021-8979. DOI: 10.1063/5.0046878.
- [17] ISO 354:2003, “Acoustics - measurement of sound absorption in a reverberation room,” *International Organization for Standardization*, 2020.
- [18] ASTM International, “ASTM E105019 standard test method for impedance and absorption of acoustical materials using a tube, two microphones and a digital frequency analysis system,” 2019.
- [19] —, “ASTM E2611-19 standard test method for normal incidence determination of porous material acoustical properties based on the transfer matrix method,” 2019.
- [20] D. Pilon, R. Panneton, and F. Sgard, “Behavioral criterion quantifying the effects of circumferential air gaps on porous materials in the standing wave tube,” *The Journal of the Acoustical Society of America*, vol. 116, 1 Jul. 2004, ISSN: 0001-4966. DOI: 10.1121/1.1756611.
- [21] L. Shtrepi and A. Prato, “Towards a sustainable approach for sound absorption assessment of building materials: Validation of small-scale reverberation room measurements,” *Applied Acoustics*, vol. 165, Aug. 2020, ISSN: 0003682X. DOI: 10.1016/j.apacoust.2020.107304.